International Symposium
On Turbulence and Shear Flow
Phenomena (TSFP-8)
August 28 - 30, 2013 Poitiers, France

AERODYNAMIC CONTROL OF A PITCHING AIRFOIL USING DISTRIBUTED ACTIVE BLEED

John M. Kearney and Ari Glezer
Woodruff School of Mechanical Engineering
Georgia Institute of Technology
Atlanta, Georgia, USA 30332-0405

ABSTRACT

The aerodynamic forces and moments on a static and a dynamically pitching 2-D airfoil model are controlled in wind tunnel experiments using distributed active bleed. Bleed flow on the suction surface downstream of the leading edge is driven by pressure differences across the airfoil surfaces and is regulated by low-power louver actuators. The bleed interacts with cross flows to effect time-dependent variations of the vorticity flux and thereby alters the local flow attachment, resulting in significant changes in lift and pitching moment at static pre- and post-stall angles (over 50% increase in baseline post-stall lift). The flow field over the airfoil is measured using high-speed (2000 fps) PIV, resolving the dynamics and characteristic time-scales of vorticity production and advection that are associated with transient variations in lift. It is shown that bleed actuation can improve the lift hysteresis and negative damping characteristics during oscillatory pitching by affecting the shedding of the dynamic stall vortex and the ensuing flow attachment during the downstroke.

I. OVERVIEW

The use of passive bleed through porous surface segments for aerodynamic flow control by exploiting inherent pressure differences over surfaces of moving bodies has been explored in a number of earlier investigations. The interaction of the ejection or suction with the cross flow can result in a local modification of the pressure distribution, alteration of the flow over the surface, and global changes in aerodynamic forces. Examples include aerodynamic maneuvering forces (Hunter et al., 2001), tip vortex control (Han and Leishman, 2004), and mitigation of flow separation (Lopera, Ng, and Patel, 2004).

Kearney and Glezer (2011, 2012) demonstrated the effectiveness of *active*, distributed bleed for controlling the pre- and post stall aerodynamic forces and moments on both static and dynamically pitching airfoils and showed how the bleed can affect vorticity production, accumulation, and shedding. When an airfoil undergoes time-periodic pitch oscillations beyond its static stall angle, the flow adjacent to its suction surface is dominated by the formation, advection, and ultimate shedding of the dynamic stall vortex, which can cause structural vibrations and flutter (Johnson and Ham, 1972, Carta and Carlson, 1973, McCroskey et al., 1976, Ericsson and Reding, 1988, and Lee and Gerontakos, 2004). A number of numerical and experimental investigations have sought to reduce or eliminate the variations in lift and negative damping associated with dynamic stall using active flow control (e.g. steady blowing, Weaver et al. 1996; synthetic jets, Wu et al., 1998, Greenblatt and Wygnanski, 2001, and Florea and Wake, 2003; combustion actuation, Woo and Glezer, 2010; plasma actuation, Post and Corke, 2006). Several of these investigations indicated that periodic excitation of the separating shear layer can increase the steady and unsteady stall angles and the post-stall lift and reduce the unfavorable direction of the induced pitching moment. In contrast to these approaches, which require considerable actuation power, actuation derived from the regulation of aerodynamic bleed driven by pressure differences across lifting surfaces requires relatively little power.

The present investigation builds on earlier findings of Kearney and Glezer and focuses on time-resolved interactions between the bleed and the cross flow over a static and a pitching airfoil, with specific emphasis on the effects of bleed on the formation and shedding of the dynamic stall vortex.

II. EXPERIMENTAL SETUP AND PROCEDURES

The present investigation is conducted in a small, low-speed ($3 < U_\infty < 35$m/s) closed-return atmospheric wind tunnel, having a rectangular test section measuring 25 x 47 x 132cm with optical access from all sides. The VR-7 airfoil model has a 20cm chord, maximum thickness of 0.12c, and spans the almost the entire width of the test section (24 cm). It is mounted using shafts connected to compression endplates to minimize flow three-dimensionality over the airfoil. The model is mechanically isolated from the test section and is mounted on a shaft centered through $x/c = 0.25$. The shaft is suspended between two external load cells that measure the lift and drag force and the pitching moment with resolutions of 0.002N/mV and with maximum frequency response of 500Hz. The load cells are attached to mechanical couplings on each side of the tunnel that are each driven by a servo motor, such that both motors are synchronized for dynamic pitching of the airfoil. The mechanical pitch system is mounted on an external frame that surrounds the test section. The current system can pitch the model time-harmonically at frequencies in excess of 25 Hz (corresponding to reduced frequency of up to $k = \omega c/2U_\infty \approx 1$). High-speed PIV measurements (2000 fps) are obtained using a 1280 x 800 pixel, 12-bit CCD camera and an Nd:YLF laser. Cross-stream measurement are taken at mid span within the streamwise domains $0 < x < 0.6c$ and $0 < x < 1.25c$ (magnifications of 10 and 5 pixels/mm, respectively).

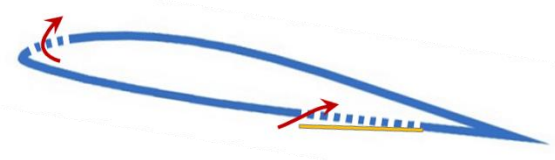

Figure 1. Bleed through the VR-7 airfoil from the pressure surface near the trailing edge to the suction surface near the leading edge.

The airfoil model is fabricated using stereolithography (SLA) and is designed to include several spanwise rows of bleed passages through the pressure and suction surfaces. The bleed ports are arranged on a surface grid that forms the skin such that each spanwise row is comprised of 16 ports each 10 mm wide, and their streamwise extent increases with streamwise distance from the leading edge from 2.0 mm (at $x/c = 0$) to 2.5 mm (at $x/c = 0.95$). The large-area, low-resistance surface grids are open to the inner volume of the model (Figure 1). The bleed configuration discussed in the present work leverages the relatively high pressure region on the pressure surface near the trailing edge to force flow through the interior volume and to a low pressure domain on the suction surface near the leading edge ($0.03 < x/c < 0.04$). An array of planar piezoelectric louvers embedded across the airfoil's pressure-side exterior span can be actuated at frequencies above 150Hz to enable air flow between high and low pressure regions along the surface of the airfoil. Time-dependent actuation waveforms are synthesized using the laboratory computer and external amplifiers and can maintain the louvers at an offset from the airfoil surface, allowing for continuous and/or dynamic levels of bleed. As noted by Kearney and Glezer (2012), the static displacement of the louvers (characterized by the fractional opening, Λ) varies linearly with the applied voltage, and the effects of the louvers' presence on the aerodynamic characteristics of the airfoil in the absence of bleed (i.e. when the bleed passages are sealed), assessed from load cell measurements, results in minimal interference and changes in aerodynamic forces.

III. BLEED ACTUATION AT STATIC ANGLES

Previous investigations (Kearney and Glezer, 2011, 2012) have demonstrated that louver-regulated time-invariant and time-periodic bleed actuation can effect significant changes in the time-averaged aerodynamic forces over a broad range of angles of attack. Figure 2 shows the variations of C_L, C_M, and C_D with angle of attack for the baseline (sealed) airfoil, using time-invariant bleed at $\Lambda = 1$, and in the presence of continuous time-periodic bleed at $St_{act} = f_{act}c/U_\infty = 1.1$ ($f_{act} = 83$Hz) and Re = 190,000. Time-invariant bleed does not significantly affect C_L below $\alpha = 7°$ but spoils the lift between $8° < \alpha < 22°$, with a maximum decrease relative to baseline levels of $\Delta C_L/C_{L0} = -0.32$ at $\alpha = 15°$. Time-periodic actuation can lead to flow attachment that is accompanied by a significant increase in lift near the stall angle ($\Delta C_L/C_{L0} = 0.20$ at $\alpha = 17°$) and can maintain elevated lift levels as α increases. For this bleed configuration, a maximum post-stall increment in lift of $\Delta C_{L,max}/C_{L0} = 0.51$ is observed at $\alpha = 19°$. It is noted that bleed actuation may be operated time-periodically with respect to a fractional opening $0 < \lambda < \Lambda$, thereby enabling continuous variation of C_L between the maximum time-periodic value and the minimum time-invariant value at a given angle.

Time-periodic and time-invariant bleed also induce slight nose-up pitching moments about $c/4$ relative to the baseline at low to moderate angles of attack ($0° < \alpha < 11°$). As flow begins to separate near the trailing edge ($\alpha = 10°$), bleed actuation generates a nose-down moment of increasing magnitude; by the static stall angle ($\alpha = 17°$), $\Delta C_M/C_{M0} = -1.10$ and -1.47 for time-periodic and time-invariant bleed, respectively. Variations in drag due to bleed are small below $\alpha < 12°$ and appear to reach levels that are commensurate with the baseline airfoil's stall beginning at $\alpha = 14°$ for time-invariant and $\alpha = 16°$ for time-periodic bleed.

The effects of bleed on the flow field of the baseline airfoil are shown in Figure 3 using raster plots of spanwise vorticity concentrations coupled with velocity vectors at $\alpha = 16°$ for the baseline airfoil (Figure 3a) and in the presence of bleed actuation (time-invariant, $\Lambda = 1$, Figure 3b, and time-periodic, $St_{act} = 1.1$, Figure 3c). Figure 3a indicates attached flow through $x/c \approx 0.45$ followed by a separation domain ($0.5 < x/c < 1$) that is bounded by a free shear layer and a thin layer of counter-clockwise vorticity induced by the recirculating flow along the airfoil's surface. In Figure 3b, the bleed flow interacts with the cross flow to initiate earlier separation at $x/c \approx 0.2$ such that the separating shear layer is vectored away from the airfoil at an angle of approximately 10° with respect to the free stream. The CCW vorticity layer over the airfoil's

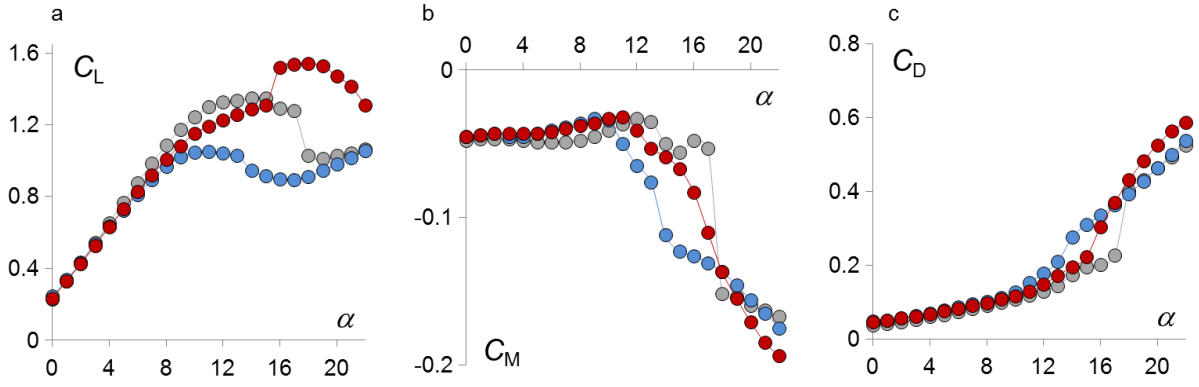

Figure 2. Variation of C_L (a), C_M (b), and C_D (c) with static angle of attack for the baseline airfoil (●), time-invariant bleed at $\Lambda = 1$ (●), and time-periodic bleed (●) at $St_{act} = 1.1$ with the bleed outlet at $0.03 < x/c < 0.04$.

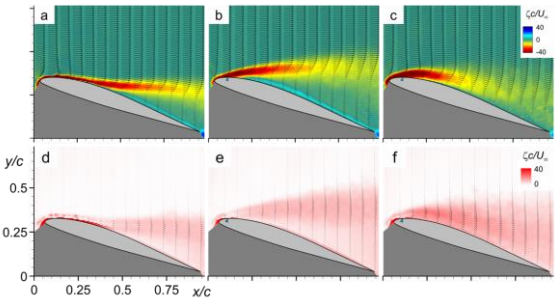

Figure 3. Time-averaged spanwise vorticity contours and velocity vectors at α = 16° for flow over the baseline airfoil (a), with Λ = 1 (b), and with time-periodic actuation at St_{act} = 1.1 (c). Corresponding RMS deviations are shown in frames (d – f).

surface intensifes, indicating a stronger recirculation domain. The increased separation domain also results in a significant reduction in lift from C_L = 1.30 to 0.90. The characteristic frequency of the time-periodic bleed actuation (St_{act} = 1.1, Figure 3c) is selected to be within the receptivity range of the baseline flow and leads to nearly-complete flow attachement (there is no evidence of recirculation near the trailing edge) that is accompanied by a considerably thicker and more curved vorticity layer through the midchord compared to the baseline airfoil, and by an increase in lift to C_L = 1.52. The intensity and cross-stream extent of the RMS fluctuations of spanwise vorticity concentrations (Figures 3d, e, and f), particularly in the presence of time-periodic bleed, indicates that the attachement is associated with the time-varying transport of vorticity concentrations near the surface.

The interaction between continuous time-periodic bleed flow and the cross-stream leads to time-periodic formation of large-scale vortices that contribute to the accumulation of CW vorticity over the airfoil and induce time-periodic flow attachment, and thereby a net increase in lift during the actuation cycles or in the time-averaged lift. The mechanism by which this process occurs is illustrated in Figure 4 using a sequence of instantaneous PIV images following the onset of bleed actuation when the flow is subjected to contiunuous, time-periodic actuation at St_{act} = 1.1 (cf. Figure 3c). Although the flow over the baseline airfoil is attached through midchord, time-periodic bleed induces periodic local separation and reattachment in the vicinity of the bleed outlet. At the onset of bleed from the outlet (Figure 4a, t/T_{act} = 0), the instantaneous local separation occurs near x/c = 0.12, and a band of CW vorticity extends into the cross flow with a concentrated layer of CCW vorticity beneath it. The disruption of the locally-separated vorticity layer by the bleed flow results in the formation of a concentration of CW vorticity (Figure 4b, t/T_{act} = 0.12) that thins the vorticity layer downstream, forming a braid-like domain (Figure 4c, t/T_{act} = 0.25). This vortex continues to grow while slowly advecting downstream ($U_{celerity}/U_\infty \approx 0.35$) and becomes disconnected from the surface vorticity layer upstream as it entraines CCW vorticity from underneath (Figures 4d-f, t/T_{act} = 0.37 to 0.62), while the CW surface vorticity layer upstream remains *fully attached*. As shown in Figures 4g and h (t/T_{act} = 0.75, 0.87), the CW vortex increases in scale (its diameter is about 0.3c by x/c = 0.5) while the surface CW vorticity layer continues to migrate downstream and remain attached.

The data in Figures 4a-h suggest that the surface vorticity layer upstream of the isolated, large scale vortex remains attached due to induced motions from the CCW vorticity concentration in the upstream portion of the isolated vortex (e.g., Figures 4e-g). It is remarkable that these unsteady motions are able to overcome the

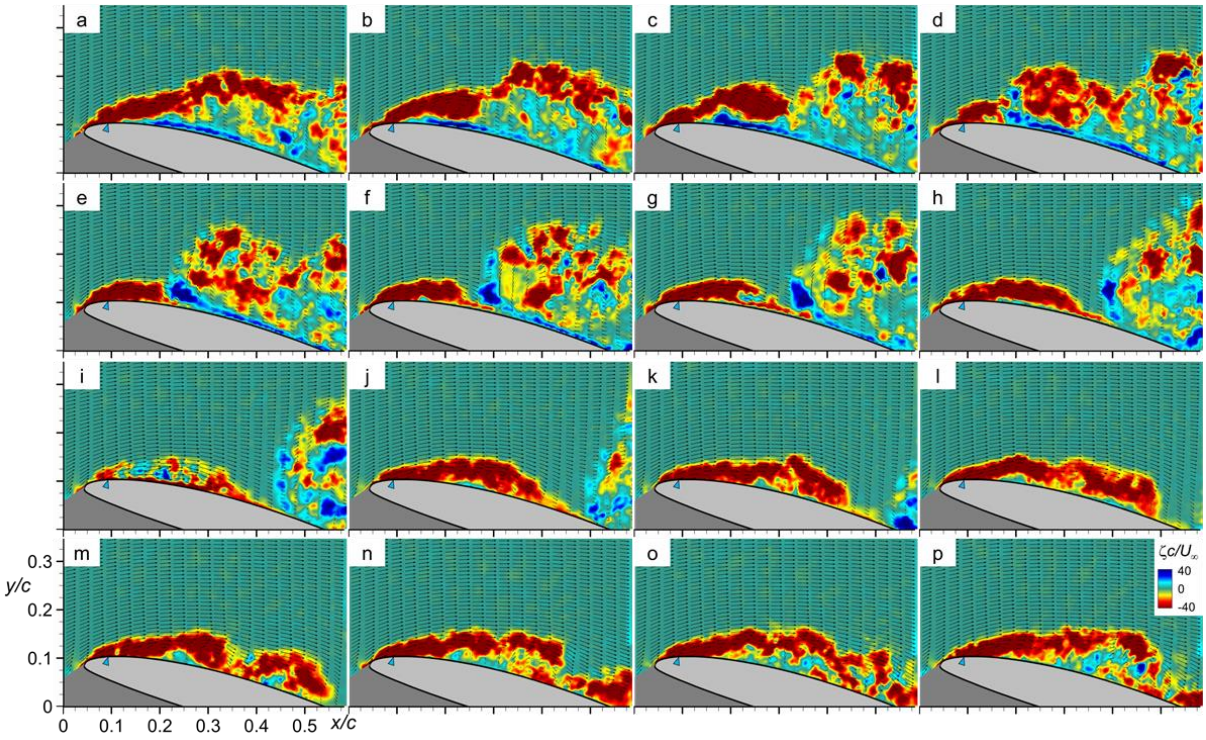

Figure 4. Instantaneous spanwise vorticity contours and velocity vectors following bleed onset during the time-periodic bleed actuation cycle at St_{act} = 1.1 and α = 16°: t/T_{act} = 0 (a), 0.12 (b), 0.25 (c), 0.37 (d), 0.50 (e), 0.62 (f), 0.75 (g), 0.87 (h), 1 (i), 1.12 (j), 1.24 (k), 1.37 (l), 1.49 (m), 1.62 (n), 1.74 (o), and 1.87 (p).

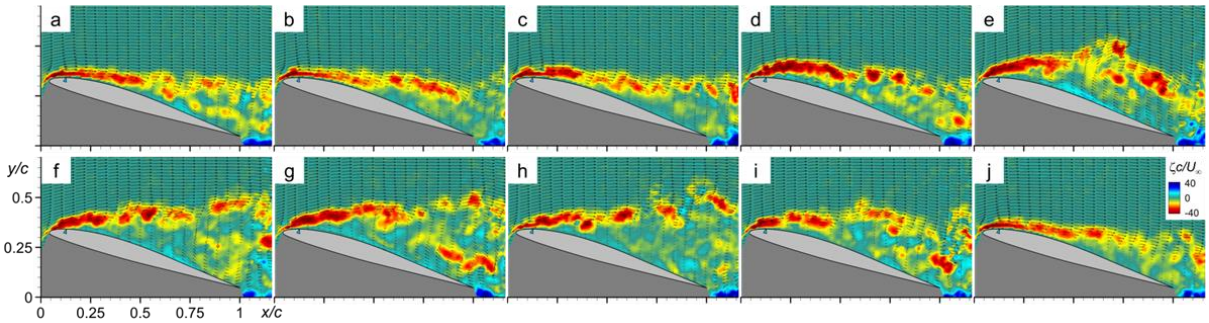

Figure 5. Instantaneous spanwise vorticity contours and velocity vectors for flow over the airfoil at $\alpha = 16°$ during the onset and termination of bleed. Timing of the frames corresponds to the timing of the measurements and actuation waveform shown in Figure 8: $t/T_{conv} = 6$ (a), 8 (b), 10 (c), 11 (d), 13 (e), 16 (f), 23 (g), 25 (h), 26 (i), and 29 (j).

nominally-adverse local pressure gradient on the suction surface of the airfoil. Furthermore, the data in Figure 4 indicate that the increase in lift as a result of the actuation is associated in part with the time-periodic formation and slow advection of the large-scale isolated CW vortex (that is reminescent of a dynamic stall vortex, although the airfoil is stantionary). The periodic shedding of this vortex is also responsible for a momentary decrease in lift, although the cycle-averaged lift is clearly higher than that of the baseline flow (cf. Figure 2a).

As noted above, the actuation frequency was selected to be within the receptivity range of the baseline flow (based on measurements of the global lift forces). However, the present PIV measurements indicate that the characteristic time constant that is associated with the attachement of the flow is actually *longer* than the actuation period. The onset of the next bleed cycle is shown in Figure 4i ($t/T_{act} = 1$). Although the bleed flow disrupts the surface vorticity layer near the leading edge, this effect seems to be minimal in Figures 4j-l ($t/T_{act} = 1.12$ to 1.37), and may be responsible for the appearance of a local breakup in Figures 4m and n ($t/T_{act} = 1.49$ and 1.62, respectively). Perhaps the most prominent feature in Figures 4o and p ($t/T_{act} = 1.74$ and 1.87, respectively) is the onset of separation of the surface vorticity layer before it interacts again with the bleed actuation at $t/T_{act} = 2$ (corresponding to Figure 4a).

The PIV data in Figure 4 indicate that the actuation frequency period is approximately half the characteristic period of the large-scale induced flow attachment following an actuation pulse that is commnesurate with the dynamics of the flow relaxation. Therefore, when the actuation is applied at $St_{act} = 0.53$, the time-averaged lift is $C_L = 1.46$ compared with 1.52 at $St_{act} = 1.1$ (in fact, measurements of the variation of the lift with actuation frequency indicate that the lift is nearly invariant for $0.53 < St_{act} < 1.60$ and begins to decrease monotonically for $St_{act} < 0.53$).

The transient effects of the onset and termination of bleed actuation on the lift and pitching moment are investigated with step changes in bleed using simultaneous PIV (Figure 5) and load cell (Figure 6) measurements. Note that the timing of the PIV frames in Figure 5 correspond the timing (a-j) along traces of C_L and C_M in Figure 6 (shown along with the actuation waveform). Just prior to actuation, the flow is nominally attached through the midchord (Figure 5a) with $C_L = 1.2$ and $C_M = -0.045$. Bleed actuation commences in Figure 5b ($t/T_{conv} = 8$) and interacts with the cross-stream to induce local accummulation of CW vorticity, and within $3T_{conv}$ (Figure 5d, $t/T_{conv} = 11$), C_L increases to 1.3. It also appears that actuation leads to an increase in the suction pressure aft of $c/4$ that is manifested by an increase in the nose-down pitching moment ($C_M = -0.090$). The subsequent formation and advection of a large-scale vortex over $2T_{conv}$ (Figure 5e), as discussed in connection with Figure 4, enhances the accumulation of clockwise vorticity and increases C_L to a maximum of 1.45 and the the nose-down moment to $C_M = -0.25$. Because C_M is measured relative to $c/4$, it peaks when the vorticity concentration convects over the trailing edge, i.e. slightly after ($\Delta t/T_{conv} = 0.15$) the occurance of the peak in lift, which depends on the pressure distribution near the leading edge.

It should be noted that unlike the actuation in Figure 4 (where the actuation cycle terminates after $0.9T_{conv}$), the bleed continues ($\Lambda = 1$) in Figures 5e-h and leads to

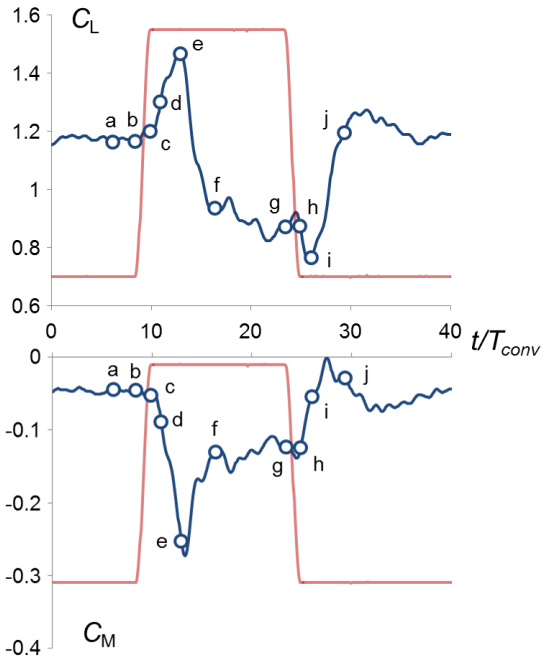

Figure 6. Measured variation in lift and pitching moment (—) in response to step changes in bleed actuation level between $\Lambda = 0$ and 1 (—, not scaled) at $\alpha = 16°$.

enhancement of the separation (cf. Figure 3b). After $3T_{conv}$ (Figure 5f), the vortex has convected into the wake, and the flow over the airfoil becomes fully separated, resulting in a decrease in lift and in the magnitude of the nose-down moment (C_L = 0.95, C_M = -0.13). The bleed is terminated in Figure 5h (t/T_{conv} = 25), and C_L decreases to 0.76 before flow attaches through x/c = 0.5 after $4T_{conv}$ (Figure 5j, t/T_{conv} = 29), and C_L and C_M relax to their original levels.

The transient increase in lift can be exploited for a sustained increase by repeated actuation as demonstrated, for example, in connection with Figure 4.

IV. BLEED ACTUATION DURING PITCH OSCILLATIONS

The recent investigations of Kearney and Glezer (2012) demonstrated that bleed actuation can lead to reductions in lift hysteresis while affecting the evolution of the dynamic stall vortex, and can also reduce pitch instability (or negative pitch damping). Figure 7 shows measurements of $C_L(\alpha)$ and $C_M(\alpha)$ that are acquired phase-locked to the airfoil's time-periodic pitch oscillations (k = 0.04) over 14° < α < 22°. The traces are shown for the baseline airfoil (gray) and in the presence of continuous time-periodic bleed actuation (St_{act} = 1.1, red) where the dashed lines indicate the downstroke segment of the cycle. The buildup and convection of the dynamic stall vortex that is evidenced by the peak in baseline lift (C_L = 1.67 at α = 19.4°) is followed by a period of reduced lift during which the airfoil is stalled until α = 17° on the downstroke (C_L = 0.93), when the flow reattaches and lift is restored. Furthermore, the baseline airfoil exhibits C_M stall when the dynamic stall vortex begins its streamwise advection, which is accompanied by a shift in the center of pressure and a nose-down moment at α = 18° on the upstroke. As a result, negative pitch damping occurs for 17° < α < 19.4° (during which the airfoil extracts energy from the flow, Liiva, 1969). The negative peak in pitching moment (C_M = -0.26) occurs at α = 19.7°, after the maximum lift (α = 19.4°). Such a phase lag between extrema of C_L and C_M was also observed in earlier studies (e.g. Carr, McAlister, and McCroskey, 1977; Weaver, McAlister, and Tso, 1996) and arises because the low pressure associated with the dynamic stall vortex generates maximum lift as it convects near the midchord and maximum (nose-down) moment as it passes over the trailing edge.

Bleed actuation leads to several changes in baseline flow. The advection and shedding of the dynamic stall vortex begins earlier in the pitch cycle while the magnitude of maximum induced lift is somewhat diminished (C_L = 1.59 at α = 18°), resulting in a less severe moment stall earlier in the cycle (α = 15.8°). Because several bleed actuation pulses occur during the upstroke, a secondary moment stall appears at α = 18.9°, indicating transient reattachment followed by the advection of another vortex similar to the dynamic stall vortex. In addition, the hysteresis associated with separated flow on the downstroke is almost completely eliminated (e.g., C_L = 1.38 at α = 17°). Bleed actuation also suppresses the negative peak in pitch observed in the baseline, and there is little or no indication of negative damping.

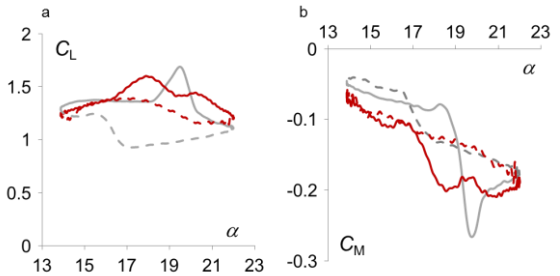

Figure 7. Variation of $C_L(\alpha)$ (a) and $C_M(\alpha)$ (b) for the baseline (—) airfoil and in the presence of time-periodic bleed (St_{act} = 1.1, —) during sinusoidal pitching at k = 0.04. Downstroke motion is shown using dashed lines.

High-speed PIV measurements over the airfoil during the pitch cycle reveal the flow mechanisms associated with the reduced hysteresis in the presence of time-periodic bleed. Figure 8 shows time sequences of the velocity fields and spanwise vorticity concentrations for the baseline airfoil (a-c) and in the presence of time-periodic bleed (d-f) during the pitch downstroke through α = 18° (Figures 8b and e). In the absence of actuation, the separated shear layer of the baseline airfoil exhibits regular advection of concentrations of clockwise vorticity throughout the time sequence, but no specific structures appear to be locked to the motion. The lingering of the separation during the downstroke results in lower lift compared to upstroke (cf., Figure 7).

The lift improvement in the presence of bleed actuation (St_{act} = 1.1, actuation period of $0.9T_{conv}$) is a result of the interaction between the bleed and the unsteady separated shear layer (similar to the mechanism discussed in connection with Figure 4). The sequence of images (Figures 8d-f) show the presence of a large-scale CW vortex upstream of the trailing edge (near x/c = 0.85 in 8d), that is absent in the baseline (unactuated) flow. This vortex resulted from an earlier bleed pulse (at t/T_{conv} = 17.6 relative to the onset of downstroke). The next actuation pulse (Figure 8d, t/T_{conv} = 18.5) leads to the

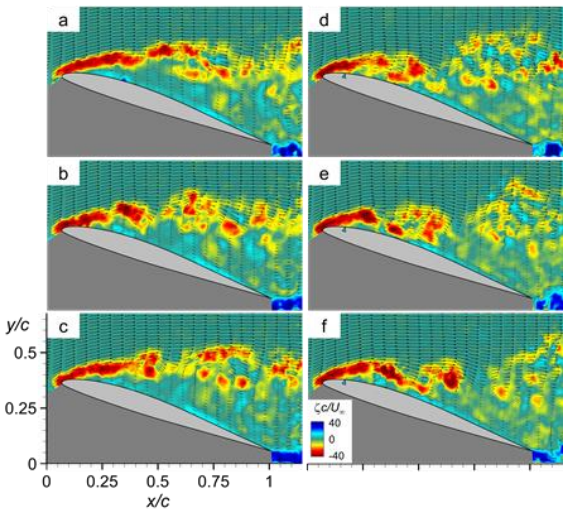

Figure 8. Instantaneous flow over the baseline airfoil (a-c) and the bleed-actuated airfoil (St_{act} = 1.1, d-f) during pitch downwards through α = 18° at k = 0.04. Temporal spacing between frames is 2.0ms ($0.15T_{conv}$), and α = 18.0° occurs in frames b and e.

formation of a new CW vortex near the surface of the airfoil that persists as it is advected along the surface. It also appears that the CCW vorticity layer that forms on the surface and is transported upstream by the motion of the large vortex induces motions that tend to diminish the shear layer separation upstream. Considering the characteristic time constant that is associated with the transitory attachment and relaxation of the separating shear layer in response to bleed actuation, the present data indicates that the performance of the airfoil in pitch can be further improved by controlling the phase of the actuation relative to the pitch cycle.

CONCLUSIONS

Aerodynamic flow control using distributed active bleed regulated by piezoelectric louvers on a stationary and a pitching VR-7 airfoil is investigated in wind tunnel experiments. Variations in loading due to time-invariant and time-periodic bleed are measured for a range of static angles of attack and can effect increases or decreases in lift by as much as +50% and -30% relative to baseline. Bleed actuation generates small nose-up (positive) changes in pitching moment for $\alpha < 11°$ and significant nose-down moments for near-stall α. These changes are accompanied by modification of the vorticity concentrations near the leading edge bleed ports, either vectoring shear layer away from the surface to deepen stall (time-invariant bleed) or reattaching the flow and restoring lift (time-periodic bleed).

The interaction between the bleed and cross flow leads to the formation of large scale CW vorticity concentrations that are subsequently advected along the surface over 1-2T_{conv}. These vortices contribute to the flow reattachment by upstream advection of a CCW vorticity layer from the surface and to an increase in lift by accumulation of CW vorticity and changes in the vorticity flux into the near wake. Periodic repetition of bleed pulses based on characteristic time scale of transitory flow response to the onset and termination of the bleed (1-2T_{conv} per pulse) yields flow attachment and a sustained increase in lift (e.g. by as much as $\Delta C_L/C_{L0} = 0.18$ at $\alpha = 16°$).

Bleed actuation can also affect the flow over the airfoil during oscillatory pitching beyond the static stall angle by promoting attachment during the downstroke, thereby reducing lift hysteresis, and shifting the formation and shedding of the dynamic stall vortex to earlier in the pitch cycle.

At quasi-steady pitching frequencies, bleed actuation produces transient attachment following the formation and advection of the dynamic stall-like CW vortices that are triggered by the bleed actuation pulses. The vortices induce upstream advection of the CCW vorticity layer from the surface of the airfoil that reduces the extent of separation upstream of the vortex. These effects reduce the lift hysteresis and therefore increase the cycle-averaged lift. This mechanism also reduces the cyclical variation in the pitching moment, contributing to pitch stability and reducing negative pitch damping.

ACKNOWLEDGEMENT

This work is supported by the Rotorcraft Center (VLRCOE) at Georgia Tech.

REFERENCES

Carr, L. W., McAlister, K. W., and McCroskey, W. J., "Analysis of the development of dynamic stall based on oscillating airfoil experiments," NASA Technical Note D-8382, 1977.

Carta, F. O., and Carlson, R. G., "Determination of Airfoil and Rotor Blade Dynamic Stall Response," *Journal of the American Helicopter Society*, **18**, 31-39, 1973.

Ericsson, L. E., and Reding, J. P., "Fluid Mechanics of Dynamic Stall Part I. Unsteady Flow Concepts," *Journal of Fluids and Structures*, **2**, 1-33, 1988.

Greenblatt, D., and Wygnanski, I., "Dynamic Stall Control by Periodic Excitation, Part 1: NACA 0015 Parametric Study," *J. Aircraft*, **38**, 430-438, 2001.

Han, Y., and Leishman, J., "Investigation of Helicopter Rotor-Blade-Tip-Vortex Alleviation Using a Slotted Tip," *AIAA Journal*, **42**, 524-535, 2004.

Hunter, C. A. Viken, S. A., Wood, R. M., and Bauer, S. X. S., "Advanced Aerodynamic Design of Passive Porosity Control Effectors," AIAA Paper 2001-0249, 39th Aerospace Sciences Meeting, Reno, Nevada, 2001.

Johnson, W., and Ham, N. D., "On the mechanism of dynamic stall," *J. Am. Helicopter Soc.*, **17**, 36‑45, 1972.

Kearney, J. M., and Glezer, A., "Aerodynamic Control using Distributed Bleed," AIAA Paper 2012-3246, 6th Flow Control Conference, New Orleans, Louisiana, 2012.

Kearney, J. M., and Glezer, A., "Aero-Effected Flight Control Using Distributed Active Bleed," AIAA Paper 2011-3099, 41st Fluid Dynamics Conference, Honolulu, Hawaii, 2011.

Lee, T., and Gerontakos, P., "Investigation of flow over an oscillating airfoil," *J. Fluid Mech.*, **512**, 313-341, 2004.

Liiva, J., "Unsteady Aerodynamic and Stall Effects on Helicopter Rotor Blade Airfoil Sections," *J. Aircraft*, **6**, 46-51, 1969.

Lopera, J., Ng, T. T., and Patel, M. P., "Experimental Investigations of Reconfigurable Porosity for Aerodynamic Control," AIAA Paper 2004-2695, 2nd Flow Control Conference, Portland, Oregon, 2004.

McCroskey, W. J., Carr, L. W., and McAlister, K. W., "Dynamic stall experiments on oscillating airfoils," *AIAA Journal*, **14**, 57‑63, 1976.

Post, M., and Corke, T. C., "Separation Control Using Plasma Actuators: Dynamic Stall Vortex Control on Oscillating Airfoil," *AIAA Journal*, **43**, 3125-3135, 2006.

Weaver, D., McAlister, K. W., and Tso, J., "Suppression of Dynamic Stall by Steady and Pulsed Upper-Surface Blowing," NASA Technical Paper 3600, 1996.

Woo, G., and Glezer, A., "Transient Control of Separating Flow over a Dynamically Pitching Airfoil," AIAA Paper 2010-861, 48th Aerospace Sciences Meeting, Orlando, Florida, 2010.

Wu, J.-Z., Lu, X.-Y., Denny, A. G., Fan, M., and Wu, J.-M., "Post Stall Flow Control on an Airfoil by Local Unsteady Forcing," *J. Fluid Mech.*, **371**, 21-58, 1998.